

# Sequential Forecasting of 100,000 Points

Xinshuo Weng<sup>1</sup>, Jianren Wang<sup>1</sup>, Sergey Levine<sup>2</sup>, Kris Kitani<sup>1</sup>, and Nicholas Rhinehart<sup>2</sup>

<sup>1</sup> Robotics Institute, Carnegie Mellon University, USA  
{xinshuow,jianrenw,kkitani}@cs.cmu.edu

<sup>2</sup> Department of Electrical Engineering and Computer Sciences, University of California, Berkeley, USA  
{svlevine,nrhinehart}@eecs.berkeley.edu

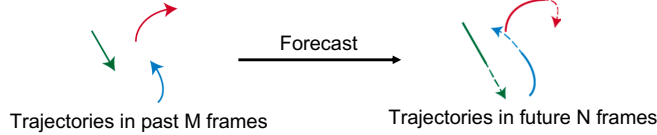
**Abstract.** Predicting the future is a crucial first step to effective control, since systems that can predict the future can select plans that lead to desired outcomes. In this work, we study the problem of future prediction at the level of 3D scenes, represented by point clouds captured by a LiDAR sensor, i.e., directly learning to forecast the evolution of >100,000 points that comprise a complete scene. We term this Scene Point Cloud Sequence Forecasting (SPCSF). By directly predicting the densest-possible 3D representation of the future, the output contains richer information than other representations such as future object trajectories. We design a method, SPCSFNet, evaluate it on the KITTI and nuScenes datasets, and find that it demonstrates excellent performance on the SPCSF task. To show that SPCSF can benefit downstream tasks such as object trajectory forecasting, we present a new object trajectory forecasting pipeline leveraging SPCSFNet. Specifically, instead of forecasting at the object level as in conventional trajectory forecasting, we propose to forecast at the sensor level and then apply detection and tracking on the predicted sensor data. As a result, our new pipeline *can remove the need of object trajectory labels* and enable large-scale training with unlabeled sensor data. Surprisingly, we found our new pipeline based on SPCSFNet was able to outperform the conventional pipeline using state-of-the-art trajectory forecasting methods, all of which *require future object trajectory labels*. Finally, we consider the evaluation of the entire trajectory forecasting pipeline. Most prior works separate the evaluation of trajectory forecasting from the evaluation of detection and tracking, which cannot evaluate the entire pipeline. We propose a new evaluation procedure and two new metrics to measure end-to-end performance of the trajectory forecasting pipeline to serve as an important complement to existing trajectory forecasting evaluation. Our code will be made publicly available at <https://github.com/xinshuoweng/SPCSF>.

**Keywords:** point cloud, trajectory forecasting

## 1 Introduction

Forecasting the future is crucial in applications such as assistive robots [27,43,25] and autonomous driving [41,62,7,50], as the ability to forecast is often the first step toward planning and control [50,70,59,19]. Prior forecasting tasks, such as

## Object Trajectory Forecasting (Prior Work)



## Scene Point Cloud Sequence Forecasting (Ours)

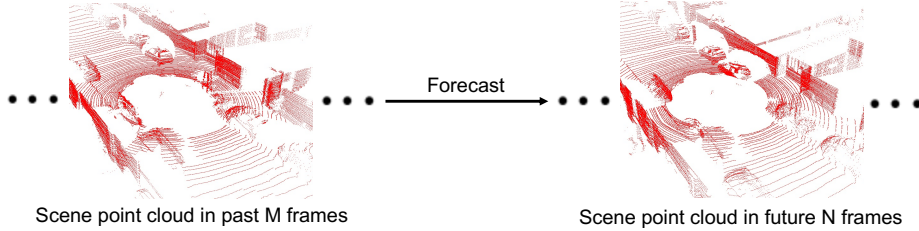


**Fig. 1: (Top) object trajectory forecasting:** given the object trajectories in past  $M$  frames, the goal is to predict the object trajectories in future  $N$  frames. **(Bottom) Scene Point Cloud Sequence Forecasting:** given 3D point clouds for an entire scene in past  $M$  frames, the goal is to predict a sequence of future scene point clouds.

trajectory forecasting and activity forecasting, focus on object-level forecasting. Specifically, trajectory forecasting [53,1,51,21,32,50,49] predicts a sequence of positions for objects of interest, and activity forecasting [31,34,48] classifies future actions of agents into pre-defined action categories. These forecasting tasks only predict sparse information about the objects, and ignore everything else such as the scene with rich information. Also, to train modern learning-based models for object-level forecasting tasks, object labels are typically required, which are costly to obtain in 3D space [3,5,10], and may not be accurate [13]. Other forecasting tasks such as video forecasting [61,18,26,44,47,14], although performs forecasting at the sensor level for an entire scene and does not require the object labels, is a 2D forecasting task and might be inefficient for application requires 3D data.

We seek a forecasting task that (1) predicts the densest-possible 3D representation (i.e. a point cloud) of the future, which contains rich information about the scene and objects; (2) requires no human annotation in order to train at a large scale. e.g., ground truth can be cheap and accurate observations captured by a LiDAR sensor. We term this task Scene Point Cloud Sequence Forecasting (SPCSF), which is to forecast a sequence of point clouds for an entire scene given past point clouds. We illustrate the difference between traditional object trajectory forecasting task and the proposed SPCSF task in Fig. 1.

To solve the proposed SPCSF task, we present the SPCSNet, which employs an LSTM [22] autoencoder model and is end-to-end trainable. To leverage the mature 2D Convolutional Neural Networks (CNNs) while preserving 3D structure of the LiDAR point cloud, we use the range map representation [4] in our best SPCSNet model. We use the raw LiDAR point cloud data from the KITTI [20] and NuScenes [5] datasets for training and evaluation, showing that

our SPCSFNet can reliably forecast the future point clouds in three seconds and outperform competitive baselines that we devised from existing techniques.

To show that our SPCSF can benefit existing downstream tasks such as trajectory forecasting, we present a new trajectory forecasting pipeline with state-of-the-art performance based on our SPCSFNet. Conventional pipelines forecast the trajectories at the object level, assuming that the detection and tracking are performed beforehand and can provide past object trajectories. Instead, our proposed trajectory forecasting pipeline performs the forecasting at the sensor level using SPCSFNet. Then 3D detectors and trackers are used on the predicted future point clouds to obtain future object trajectories. We believe that our new pipeline has two advantages: (1) by inheriting the advantage of SPCSF, we can remove the need of object trajectory labels and leverage the large-scale training to improve the performance; (2) as the possible future location of each point is constrained by the nearby points, forecasting at the sensor level for a dense 3D point cloud can lead to reduced uncertainty of the future and higher accuracy in long-horizon prediction. We will justify this in the experiments.

In terms of evaluation, prior work on trajectory forecasting often focuses on evaluating the performance of forecasting only, leaving the evaluation of detection and tracking separately. Although this per-module evaluation is important, it lacks the ability to assess the entire trajectory forecasting pipeline. In this work, we propose a new evaluation procedure along with two new metrics that can account for errors from all three modules. We believe that the new evaluation is also important in practice as the performance of forecasting highly depends on its upstream module (i.e., detection and tracking) and we are interested in the end-to-end performance for the entire system pipeline.

Our contributions are summarized as follows:

1. **a new task, Scene Point Cloud Sequence Forecasting**, which predicts the densest-possible future and does not require any human annotation;
2. **an effective approach for SPCSF**, deemed SPCSFNet, that outperforms competitive approaches we devised from S.O.T.A. techniques;
3. **a new trajectory forecasting pipeline**, that requires no trajectory labels and outperforms traditional trajectory forecasting pipeline with S.O.T.A. forecasting modules that require object trajectory labels;
4. **new evaluation procedure and metrics** that can evaluate the entire trajectory forecasting pipeline and account for the error from all modules.

## 2 Related Work

**Forecasting Tasks.** Prior tasks can be mostly categorized into trajectory forecasting, activity forecasting, and video forecasting. Trajectory forecasting works [1,21,32,54,24,29,36,50,49,11,37,66] predict a sequence of ground positions of target objects in the future. Activity forecasting [31,6,34,48] predicts person’s future actions (such as walking and running). Both trajectory forecasting and activity forecasting are object-level forecasting, which (1) require the object labels; (2) only predict sparse information about the objects. In contrast, our proposed SPCSF predicts the densest-possible 3D representation (*i.e.*, point cloud) of the future and does not require any human annotation for object labels.

Similar to our SPCSF, video forecasting [61,18,26,44,47] also performs the forecasting at the sensor level for an entire scene. However, as video forecasting predicts the RGB images captured by a camera sensor, it only delivers 2D information about the future which might be inefficient when it comes to applications that require prediction in 3D space. Beyond forecasting RGB images, [46,42] jointly predicts the future depth images and RGB images. Although depth forecasting contains partial 3D information, depth forecasting (1) does not contain full 3D information as a depth image cannot be converted to a 3D point cloud without access to the camera matrix (2) is optimized in 2D space from the frontal view and might lose the 3D structure in the point cloud, while our SPCSF is directly optimized in 3D space and can reliably preserve the LiDAR structure as shown in the experiments. Overall, prior video and depth forecasting tasks have not been demonstrated to be useful to downstream tasks, while we show the effectiveness of our SPCSF to an existing downstream task.

**Point Cloud Generation.** As SPCSF generates the future point clouds for an entire scene, prior work on point cloud generation for a single object is closely related. [16] proposes to generate the 3D point cloud of a single object with the Chamfer distance [16] and Earth Mover’s distance [52] loss. [39,23] generate the object point cloud and then project into multiple 2D viewpoints which can be optimized with the 2D re-projection error. Beyond deterministic point cloud generation, prior work employs probabilistic framework such as flow-based models [68,57], generative adversarial networks (GANs) [56] and variational autoencoders (VAEs) [30]. Instead of generating point cloud in a single frame, [17] proposes a point-based recurrent network to generate a sequence of point cloud for one or two objects, which is about 1024 points within 5 meters of range. In contrast, our SPCSF is to generate a sequence of large-scale clouds of 100,000 points for an entire scene including all objects and background in the scene.

Despite most prior works focus on a single object, there are a few works towards point cloud generation for a scene. [4] employs VAEs and GANs to generate random scene point cloud at a single frame. Beyond unconditional generation, [58] generates the scene point cloud at a single frame conditioned on the stereo images and cheap LiDAR inputs. [3] generates the point cloud in the next frame by considering the action applied to an object in the scene. Different from [4,58,3] which generate point cloud at a single frame, SPCSF aims at generating a sequence of scene point clouds. To the best of our knowledge, SPCSF is the first that is formulated as a sequence prediction of scene point clouds.

**Trajectory Forecasting Pipeline and its Evaluation.** The goal of the trajectory forecasting pipeline is to predict where the objects will move given past sensor data (*e.g.*, LiDAR point cloud). Prior works [21,54,24,8,11,37] prove that past object trajectories can provide a strong cue for trajectory prediction. From this conclusion, conventional trajectory forecasting pipeline can be dissected into two modules: (1) a detection [41,65] and tracking [64] module to obtain past object trajectories on the past sensor data; (2) a trajectory forecasting module to predict the future trajectories based on the past trajectories. Based on this



two-step dissection, most prior works [21,54,24,8,11,37] focus on step (2) only, leaving the work in step (1) for detection and tracking community.

According to the two-step dissection, the existing evaluation of trajectory forecasting module is separate from detection and tracking module. Instead of using the tracking outputs as past trajectories, existing evaluation assumes step (1) is perfectly achieved and uses ground truth past trajectories for prediction. Different from the conventional pipeline, our proposed trajectory forecasting pipeline does not rely on the past object trajectories and performs the forecasting at the sensor level. Also, our new evaluation procedure can account for the error from detection, tracking and forecasting modules, enabling the evaluation over the entire pipeline. Although [7] has the preliminary idea about evaluating the entire pipeline, their evaluation is performed at a single operating point while our evaluation with two new metrics can summarize the performance over a set of operating points and provide more fair and convincing comparison.

### 3 Scene Point Cloud Sequence Forecasting

#### 3.1 Task Formulation

The goal of our SPCSF is to predict a sequence of future scene point cloud given a sequence of past scene point clouds. Specifically, given  $M$  frames of past scene point clouds with each frame  $S_t = \{(x, y, z)_j\}_{j=1}^{K_t}$ , where  $t \in [-M+1, \dots, 0]$  denotes the frame index,  $j \in [1, \dots, K_t]$  denotes the index of points and  $K_t$  denotes the number of points

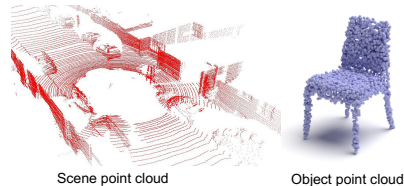


**Fig. 2:** Visual comparison of a scene point cloud to an object point cloud.

at frame  $t$ , the goal of SPCSF is to predict  $N$  frames of future scene point clouds with each frame  $S_t = \{(x, y, z)_j\}_{j=1}^{K_t}$ , where  $t \in [1, \dots, N]$ . Note that the number of points  $K_t$  can be different across frames in the past point cloud inputs (e.g., the point cloud captured by a LiDAR sensor often has different number of points across time). For simplicity, one can sample a fixed number of points in past frames and predict a fixed number of points in the future; we use  $K_t = 122,880 \forall t \in [-M+1, \dots, N]$  in order to match the normal number of points captured by a modern LiDAR (e.g., Velodyne-64).

Note that we refer the scene point cloud to as a 3D point cloud enclosing an entire scene including points belonging to objects and background, which is significantly different from many prior works on the point cloud generation of a single object. As an example, we show a scene point cloud captured by a LiDAR sensor in Fig. 2 (left) and an object point cloud in ShapeNet [9] in Fig. 2 (right).

#### 3.2 Approach: SPCSFNet

Our proposed SPCSFNet is shown in Fig. 3, which consists of four modules: (a) a shared encoder for feature extraction, (b) an LSTM for temporal modeling, (c) a shared decoder for scene point cloud generation and (4) losses. As this paper is the first work towards solving the SPCSF task, there are many unknown factors. As a result, we design our approach as a deterministic method for simplicity, despite the fact that the future is uncertain, in order to understand the

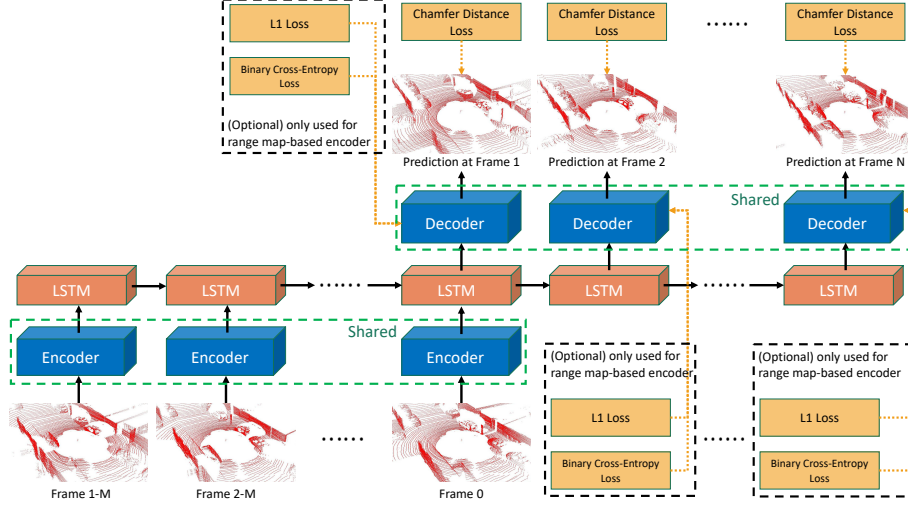


**Fig. 3: Proposed SPCSFNet.** (a) A shared encoder is used to extract features from past scene point clouds; (b) The extracted features are passed to an LSTM model to model temporal dynamics; (c) The shared decoder is employed to predict the scene point clouds; (d) Chamfer Distance loss is applied to minimize the distance between ground truth and predicted scene point clouds; (e) The L1 and binary cross-entropy losses are used to regularize the intermediate range-map outputs (Sec. 3.2).

other characteristics of the SPCSF problem. We will work towards stochastic SPCSF methods in the short future.

**Encoder.** To predict the future scene point clouds, it is important to extract useful information from the past through an effective encoder. In this work, we investigate two encoders to process the scene point clouds: (1) point-based encoder and (2) range map-based encoder, which are shown in Fig. 4 and 5.

(1) *Point-based encoder.* To process a point cloud, PointNet [45] is a straightforward choice. In Fig. 4, we adopt similar network architecture (primarily multi-layer perceptron (MLP) and max-pooling operator) as in [45] to obtain the local feature for each point and the global feature for the entire scene. To leverage the information from both local and global features, we fuse them together with feature concatenation. As the total number of points  $K$  is very large (*e.g.*, 100,000) in a LiDAR point cloud, preserving features for each individual point is not feasible throughout the network, including the subsequent LSTM and decoder. As a result, we add another MLP and a max-pooling operator to obtain a compact representation as the output feature of the encoder.

(2) *Range map-based encoder.* In addition to directly extract the feature from the point cloud, another popular approach in the literature [35,38,4,67,33] is to first transform the point cloud into a 2D representation and then use 2D CNNs for feature extraction. Although being fast and efficient, the disadvantage of most of these methods (except for [4]) is that they lose 3D structure of the point cloud due to 2D projection to bird’s eye view or frontal view, and thus not good for scene point cloud generation. As a result, we choose the range map

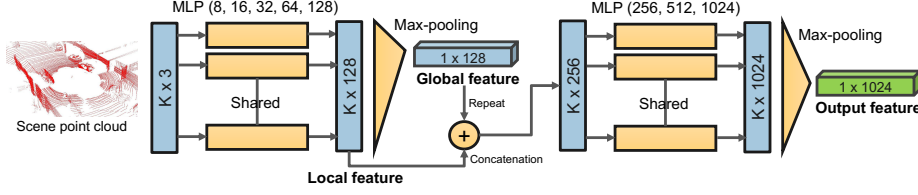


**Fig. 4: Point-based encoder.** A scene point cloud with shape of  $K \times 3$  is fed into shared MLP to obtain local feature for each point. Then a global feature is obtained by max-pooling. We then fuse the local and global features by concatenation, which is then processed by subsequent MLP and max-pooling to obtain the output feature.

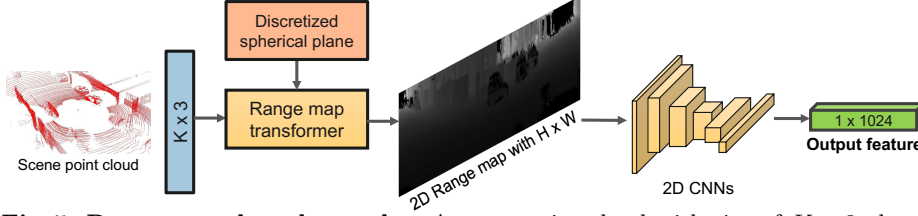


**Fig. 5: Range map-based encoder.** A scene point cloud with size of  $K \times 3$  along with a discretized spherical plane is fed into the range map transformer to obtain the 2D range map with resolution of  $H \times W$ . We use a standard 2D CNNs to extract the final output feature from the 2D range map.

representation [4], which is a special 2D representation because the 3D structure of the point cloud can be still preserved after transformed into a 2D map.

We briefly summarize the range map transformation here but refer the reader to [4] for details. Intuitively, range map representation leverages the ray-casting nature of the LiDAR point cloud and projects the points onto a 2D spherical plane. For a 3D point  $P = (x, y, z)$  in the scene point cloud with  $z$  represents the height, its coordinate in the 2D spherical plane  $Q = (\theta, \phi)$  is defined as follows:  $\theta = \text{atan2}(y, x)$ ,  $\phi = \arcsin(z / \sqrt{x^2 + y^2 + z^2})$ , where  $\theta$  is the azimuth angle and  $\phi$  is the elevation angle from the origin. Then, to convert the continuous 2D spherical plane into a discrete 2D range map with resolution of  $H \times W$ , we discretize the 2D spherical plane with a fixed number of bins ( $H$  bins along elevation axis,  $W$  bins along azimuth axis) in a pre-defined range, *e.g.*,  $\phi \in [-30^\circ, 10^\circ]$  and  $\theta \in [0^\circ, 360^\circ]$ . The range is chosen as most points captured by a normal LiDAR sensor fall into it. As a result, each bin (*i.e.*, an pixel in the range map) will cover the range of  $(\frac{40^\circ}{H}, \frac{360^\circ}{W})$  in the spherical plane, and we can easily find the nearest bin for each point  $Q = (\theta, \phi)$  as its pixel location. In order to recover the 3D coordinate of a point from its 2D spherical coordinate, knowing the azimuth and elevation angle is not enough as they only provide the direction of the point to the origin in 3D space. Therefore, we use the distance  $d = \sqrt{x^2 + y^2 + z^2}$  as the pixel value for each projected point in the 2D range map. In the case where multiple 3D points are projected to the same bin in the range map, we use their average distance  $d$  as the pixel value. For the bins that do not have any projected point, we simply fill their pixel value with zero and

will mask them out during training and inference. As a result, the range map with a resolution of  $H \times W$  still preserves the 3D information and can be easily converted back to a point cloud, although with some level of compression due to the averaging effect. Note that the range map is different from a depth map in that (1) two maps are not in a same 2D coordinate; (2) depth map needs the camera matrix in order to be converted to a point cloud while the range map can be directly converted to a point cloud; (3) depth map usually only covers the points in frontal view while range map defined above covers  $360^\circ$ .

With the input scene point cloud being transformed into a 2D range map, 2D CNNs become the natural choice to extract the feature. We show the range map-based encoder in Fig. 5. To make SPCSFNet compatible with both point-based encoder and range map-based encoder, we design the 2D CNNs in the range map-based encoder so that it can produce an output feature with the same dimension of 1024. Besides point-based and 2D projection-based point cloud processing techniques, we have not investigated the voxelization-based technique [72,12] on the SPCSF task, which we will leave as a future direction.

**Temporal Dynamics Modeling.** As SPCSF is formulated as a sequence-to-sequence problem, we use a standard LSTM network [22] to learn the temporal dynamics of the feature and propagate into the future. Specifically, we feed the feature obtained from the encoder in past  $M$  frames to the LSTM network and predict the feature for future  $N$  frames in an autoregressive manner.

**Decoder.** To predict the scene point cloud, a decoder is needed to convert the predicted feature from LSTM to a scene point cloud. With two (point-based and range map-based) encoders carefully designed, the corresponding decoder simply follows the encoder design in a symmetric manner: (1) For the point-based decoder, we adopt similar network as in [69]. Specifically, the decoder first increases the dimensionality of the LSTM output feature to a feature with a size of  $1 \times (K \times 3)$  using MLP, and then reshape it to a scene point cloud with a size of  $K \times 3$ . (2) For the range map-based decoder, we use a 2D CNNs with all deconvolution layers to map the LSTM predicted feature back to a range map with  $H \times W$ . In addition, to deal with the holes (*i.e.*, the pixels that do not have any point) in the range map, we also predict a range mask with  $H \times W$  using a similar 2D CNNs with all deconvolution layers. Then, when we transform the predicted range map back to a scene point cloud only for the pixels that are not masked out in the predicted range mask.

**Losses.** To train the SPCSFNet, we follow recent work [69,16] on deterministic point cloud generation and use the Chamfer distance [16] loss  $L_{cd}$  to minimize the distance between ground truth and predicted scene point clouds.

In addition, when we use the range map-based encoder and decoder, we add two additional losses in order to regularize the intermediate range map outputs: (1) a  $L_1$  distance loss that minimizes the distance between the ground truth and predicted range maps; (2) a binary cross-entropy loss  $L_{bce}$  between the each pixel in the predicted and corresponding ground truth range mask. All three losses are applied to all future  $N$  frames. As a result, our full objective function is:

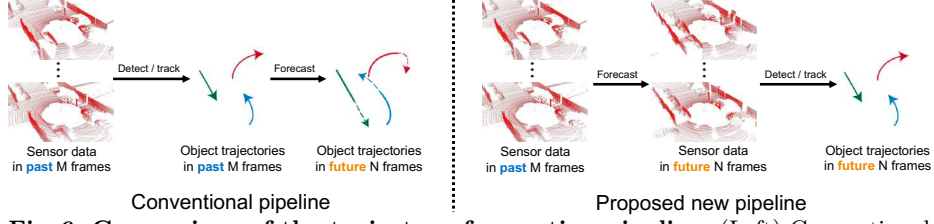


**Fig. 6: Comparison of the trajectory forecasting pipeline.** (Left) Conventional pipeline detects and tracks objects on the past sensor data and then forecasts the trajectories into future. (Right) Our proposed new pipeline first forecasts the sensor data and then detects and tracks objects in the predicted future sensor data.

$$\mathcal{L} = \sum_{i=1}^N \mathcal{L}_{cd}^i + \lambda_1 \mathcal{L}_1^i + \lambda_2 \mathcal{L}_{bce}^i, \quad (1)$$

where  $L_1$  and  $L_{bce}$  are used only when range map-based encoder-decoder is used.

## 4 New Trajectory Forecasting Pipeline

As mentioned in related work, conventional trajectory forecasting pipeline is often dissected into two steps as shown in Fig. 6 (left): (1) a detection and tracking module to obtain the past object trajectories on the past sensor data; (2) a trajectory forecasting module to predict the future trajectories based on the past trajectories. Note that we term the ‘trajectory forecasting pipeline’ and ‘trajectory forecasting module’ differently, where the trajectory forecasting module refers to as the step (2) only in the trajectory forecasting pipeline. Different from the conventional pipeline, we propose a new trajectory forecasting pipeline as shown in Fig. 6 (right). Specifically, we first forecast past sensor data into the future using our SPCSFNet. Then, we use the detector and tracker on the predicted future sensor data to obtain future object trajectories. Here, we only consider the scene point cloud captured by LiDAR as the sensor data.

The difference between conventional and our proposed pipeline is that we invert the order of forecasting and detection/tracking, and perform the forecasting at the sensor level instead of at the object level. We believe that this difference provides us two significant advantages: (1) our forecasting at the sensor level for a dense 3D point cloud can leverage stronger constraint. Specifically, the possible location of each point in the future is constrained by nearby points, which can lead to reduced uncertainty of where the points should be in the future and higher accuracy of the forecasting, especially for long-horizon forecasting. We will justify this in the ablation; (2) our pipeline can remove the need of trajectory labels. Conventional pipeline performing the forecasting at the object level requires the trajectory labels to train the forecasting module. In contrast, our proposed pipeline, which performs the forecasting at the sensor level, only needs the future sensor data for training and does not require object-level labels. Although some learning-based trackers in the pipeline might still need the trajectory label, we completely remove the need of trajectory labels by using a Kalman filter-based tracker [64] in our experiments which does not need training.

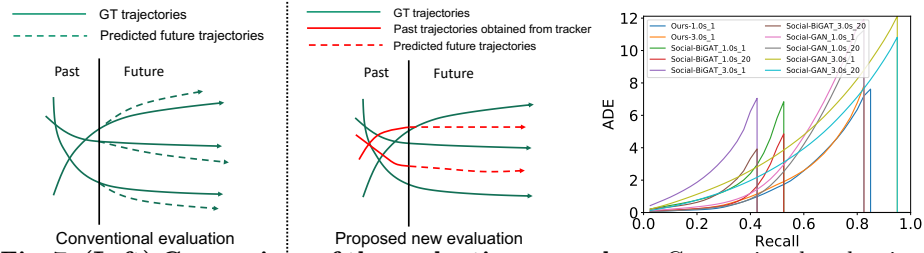


**Fig. 7: (Left) Comparison of the evaluation procedure.** Conventional evaluation uses the GT past to predict the future, which does not account for the error from detection and tracking. Our proposed evaluation uses tracking outputs as past trajectories to predict the future trajectories and the entire pipeline can be evaluated considering error from all modules. **(Right) ADE-over-recall curve.** Different methods have different recall values and it is not fair to compare the ADE of methods performing at different recalls. Therefore, integral metrics are preferred for fair comparison.

## 5 New Trajectory Evaluation Procedure and Metrics

Existing trajectory evaluation is closely related to the trajectory forecasting pipeline. As the conventional pipeline is dissected into two steps: (1) detect/track and (2) forecast, as mentioned in Sec. 4, existing evaluation is also modularized. Specifically, existing evaluation is split into two parts: (1) evaluation of the object detection and tracking, and (2) evaluation of the trajectory forecasting assuming that the GT past trajectories are given to predict future trajectories. As a result, the trajectory forecasting community focuses on step (2) and evaluates only on the forecasting part. Although this modularized evaluation procedure is useful to measure the per-module performance, it lacks the ability to validate the performance of the entire trajectory forecasting pipeline including all three modules, *i.e.*, detection, tracking, and forecasting.

To enable the evaluation of the entire pipeline, we propose a new evaluation procedure. Specifically, instead of using the GT past trajectories for future prediction, we use the tracking outputs on the past sensor data as the past trajectories. In this way, the error made in detection and tracking modules will be propagated to the forecasting module and the entire pipeline can be evaluated. We believe that, in addition to the existing per-module evaluation, our proposed evaluation is also important in practice as the performance of forecasting highly depends on its upstream module (*i.e.*, detection and tracking) and we are interested in the end-to-end performance. We illustrate the difference between the conventional and proposed trajectory evaluation procedure in Fig. 7 (left).

In addition to what past trajectories we should use, other questions to be addressed are what metrics to use and how to compute. Here, we consider the most commonly used metrics: Average Displacement Error (ADE) and Final Displacement Error (FDE), which compute the distance between each pair of future prediction and its corresponding GT. In conventional evaluation (Fig. 7 left), as the GT past trajectories are used, computing ADE and FDE is straightforward as each predicted future trajectory has its corresponding GT. However, in our proposed evaluation procedure (Fig. 7 left), computing ADE and FDE requires

additional matching step. This is because, when the tracking outputs are used as past trajectories, the correspondence between GT and predicted future trajectories is unclear. To match the predicted trajectories with GT and be able to compute the metrics, we use the Hungarian algorithm [60].

Moreover, as the proposed evaluation procedure propagates the error from detection and tracking modules to forecasting, there might be GT objects not having corresponding predicted trajectories (*i.e.*, a false negative) and thus the recall will not be 100% and also be different across methods. As an example, we show the ADE-over-recall curve computed on the KITTI dataset in Fig. 7 (right) for our method<sup>3</sup> and two baselines (see Sec. 6.2 for details). As a result, it is not fair to compare the ADE/FDE of different methods performing at a different recall. To overcome the issue, we propose two new metrics called AADE and AFDE (Average ADE and Average FDE) to summarize the performance of ADE and FDE across a set of recall values (up to a recall that all methods can reach) for a fair comparison. Specifically, AADE and AFDE are computed by integrating over ADE and FDE. Similar to existing integral metrics such as average precision [15] for detection and AMOTA for tracking [64], we approximate the integration by a summation over a discrete set of recall values.

It is important to note that our proposed trajectory forecasting pipeline can also be evaluated with the new evaluation procedure and metrics. In our new pipeline, the predicted future trajectories are obtained by running the detector and tracker on the predicted future sensor data. As a result, the predicted trajectories do not have any correspondence with the GT, and the recall will not be 100% due to the error accumulated in each module. The situation is the same as the conventional pipeline when using the new evaluation procedure. Therefore, we can fairly compare the conventional and our new trajectory forecasting pipeline based on the new evaluation procedure and metrics.

## 6 Experiments

**Dataset.** We evaluate on KITTI-Raw-Car [20] and NuScenes-Car [5], each with 156 and 1000 point cloud sequences. For KITTI, we split the train, val, and test each with 126/15/15 sequences. For NuScenes, we use the default splits.

**Implementation Details.** For the 2D CNNs in the range map-based encoder, we use nine 2D convolutional layers each followed by the batch normalization and ReLU except for the last convolutional layer. We use the range map with a size of  $(H, W) = (120, 1024)$  so that the range map can be converted to a point cloud with a similar number of points as in the raw LiDAR point cloud. We use a two-layer LSTM with the hidden feature dimension of 1024.

### 6.1 Evaluating Scene Point Cloud Sequence Forecasting

**Evaluation Metric.** We use Earth Mover’s Distance (EMD) [52] and Chamfer Distance (CD) [16] to measure the distance between two point clouds.

**Baselines.** As this paper is the first towards solving SPCSF, there is no direct baseline to compare. Therefore, we devise competitive baselines based on existing

<sup>3</sup> We denote our method for 3.0s prediction with 1 sample as Ours-3.0s\_1.



**Table 1:** Quantitative evaluation for the proposed SPCSF task on the KITTI and nuScenes datasets. Ours+Point and Ours+RM denote that we use the point-based and range map-based encoder-decoder for our method respectively.

Datasets	Metrics	Identity	GT-Ego	Est-Ego	Align-ICP	Align-[63]	SceneFlow	Ours+Point	Ours+RM
KITTI-1.0s	CD↓	12.82	5.47	9.18	6.13	6.02	3.15	1.71	<b>0.89</b>
	EMD↓	526.87	391.03	495.21	418.25	439.17	291.63	211.47	<b>128.81</b>
KITTI-3.0s	CD↓	13.31	7.91	11.31	9.14	9.57	5.08	1.95	<b>0.94</b>
	EMD↓	602.89	452.81	502.83	470.25	493.26	351.46	267.42	<b>175.54</b>
NuScenes-1.0s	CD↓	8.42	2.16	4.91	4.04	3.50	1.93	1.03	<b>0.35</b>
	EMD↓	461.63	168.37	299.13	281.53	270.81	117.41	135.94	<b>78.37</b>
NuScenes-3.0s	CD↓	10.16	2.85	6.52	7.13	5.27	3.81	1.37	<b>0.41</b>
	EMD↓	494.81	190.14	370.91	419.37	332.97	294.53	128.26	<b>91.83</b>

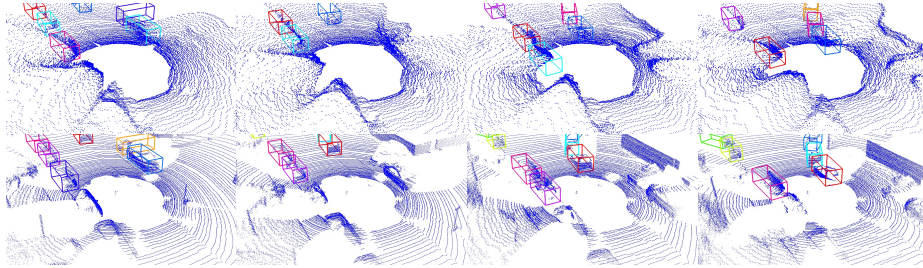


**Fig. 8: Visualization on KITTI.** (Top) Our predicted scene point cloud and tracking outputs; (Bottom) GT scene point cloud and GT box/trajectory labels. Note that KITTI dataset only has labels for object in frontal view. Also the objects color will be different in prediction and GT because the absolute IDs are different.

techniques: (1) *Identity*. We duplicate the scene point cloud from the last frame of the past to the future for  $N$  times; (2) *GT-Ego*. We use the ground truth ego-motion (rotation and translation) between adjacent past frames and compute an average motion. Then, we use the average motion to warp the last frame of past scene point cloud into the future frames; (3) *Est-Ego*. Instead of using the ground truth ego-motion, we estimate the ego-motion using [71] for warping; (4) *Align*. We use the point cloud alignment methods such as ICP [2] and Deep-ICP [63] to compute the global rigid motion between adjacent past frames and obtain the average motion for warping; (5) *SceneFlow*. We use scene flow methods such as [40] to estimate the point-wise motion between the last two frames in the past and use the motion to warp the scene point cloud into future frames. For baselines that require training, we fine-tune their models on the KITTI and nuScenes datasets for better performance.

**Setting.** We evaluate two settings for all methods: (1) observe 1.0 second past and predict the next 1.0 second; (2) observe 3.0 seconds past and predict the next 3.0 seconds. For KITTI, 1.0 and 3.0 seconds means 10 and 30 frames. For NuScenes key-frames only, 1.0 and 3.0 seconds means 2 and 6 key-frames.

**Results.** We summarize the performance for the proposed SPCSF task on the KITTI and NuScenes datasets in Table 1, where +RM and +Point denote the range map-based and point-based encoder-decoder for our method. The proposed SPCSFNet consistently outperforms all competitive baselines in both EMD and CD metrics. We believe it is because our proposed SPCSFNet (1) is designed



for sequence prediction and (2) can learn the future location for each individual point. On the other hand, the baselines are originally designed for one-frame prediction (*i.e.*, warping between two frames), leading to worse performance in long-horizon prediction. Also, most baselines can only estimate the global rigid motion and do not account for point-wise motion except for [40]. Moreover, we observe that the performance of our SPCSFNet at 1.0s and 3.0s prediction is very close. Our hypothesis is that forecasting at the sensor level for a dense 3D point cloud can possibly have a stronger constraint on future point location and reduce the certainty of the future, thus having higher accuracy for long-horizon prediction. We will justify this hypothesis in the ablation study. Also, we observe that Ours+RM performs better than Ours+Point. We believe this is because the range map preserves a better 3D structure than the point-based encoder.

**Visualization.** We visualize the results of our best SPCSF model for the KITTI-3.0s setting in Fig. 8. We plot 4 frames of results from a prediction of 30 frames with an interval of 7 frames, showing that our predicted scene point cloud reasonably reconstructs the objects and scene, and aligns well with the GT. However, the limitation is that the surface of the object points is not smooth and a few objects at a large distance are missing, which we will improve in the future work.

## 6.2 Evaluating Trajectory Forecasting pipeline

**Evaluation Metric.** We use the proposed evaluation procedure along with the proposed AADE and AFDE metrics to evaluate the conventional and our new trajectory forecasting pipeline. We do not use ADE and FDE metrics because it is not fair to compare methods that perform at different recall values.

**Baselines.** We employ different trajectory forecasting modules [21,32,8,11]<sup>4</sup> for conventional trajectory forecasting pipeline. Although [21,32] are originally proposed for predicting the trajectory of people, we adapt them to work with the car. For a fair comparison, we use the same detector [55] and tracker [64] for both our and conventional trajectory forecasting pipeline.

**Setting.** Same as evaluating SPCSF, we use the 1.0 and 3.0 seconds prediction. As trajectory forecasting modules used in the conventional pipeline performs stochastic prediction, we evaluate them by sampling 1 and 20 times. For our pipeline with deterministic SPCSFNet, it can be viewed as 1 sample. Also, we use the best SPCSFNet model trained with the range map-based encoder.

**Results.** We summarize the performance for trajectory forecasting pipeline on the KITTI and NuScenes datasets in Table 2. The proposed new pipeline outperforms conventional pipeline using different stochastic forecasting modules with 1 sample. Even when sampling 20 times for conventional pipeline, our pipeline still achieves the best performance in most settings except for the nuScenes-1.0s setting, where we are behind the Social-GAN by about 0.6 AADE and AFDE. This shows the advantage of performing forecasting at the sensor level in our new pipeline. Also, one interesting finding is that, unlike baselines which perform much worse in 3.0s prediction than in 1.0s prediction, the performance of our

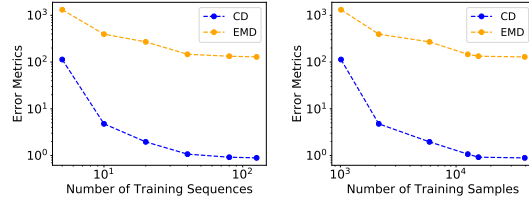
<sup>4</sup> As open-source code is not available for [32], we implement it with the best effort.

**Table 2:** Evaluation for entire trajectory forecasting pipeline on the KITTI and NuScenes datasets using the proposed evaluation procedure and metrics.

Datasets	Metrics	Samples	Conv-Social [11]	Social-GAN [21]	Social-BiGAT [32]	TraPHic [8]	Ours
KITTI-1.0s	AADE↓	1	0.792	0.524	1.099	0.470	<b>0.317</b>
		20	0.623	0.340	0.443	0.382	–
	AFDE↓	1	1.285	0.886	1.708	0.889	<b>0.405</b>
		20	1.152	0.511	0.546	0.613	–
KITTI-3.0s	AADE↓	1	1.692	1.362	2.720	1.432	<b>0.408</b>
		20	1.593	0.984	1.231	0.725	–
	AFDE↓	1	2.670	2.267	3.938	2.536	<b>0.504</b>
		20	2.385	1.512	1.405	1.118	–
NuScenes-1.0s	AADE↓	1	1.186	1.117	2.030	1.214	<b>0.821</b>
		20	0.907	<b>0.762</b>	0.826	0.881	–
	AFDE↓	1	1.490	1.310	2.337	1.563	<b>0.825</b>
		20	1.231	<b>0.763</b>	0.849	1.197	–
NuScenes-3.0s	AADE↓	1	1.794	2.224	4.954	2.417	<b>1.044</b>
		20	1.658	1.426	1.760	1.938	–
	AFDE↓	1	2.850	3.224	6.765	3.479	<b>1.043</b>
		20	2.538	1.652	1.845	2.766	–

**Table 3:** Effect of the global scene constraint.

Datasets	Metrics	w/o Scene	w/ Scene
KITTI-1.0s	CD↓	3.37	0.89
	EMD↓	261.95	128.81
KITTI-3.0s	CD↓	5.91	0.94
	EMD↓	358.16	175.54
KITTI-1.0s	AADE↓	0.845	0.317
	AFDE↓	1.593	0.405
KITTI-3.0s	AADE↓	1.347	0.408
	AFDE↓	2.984	0.504

**Fig. 9:** Error vs. amount of training data.

pipeline does not decrease significantly in 3.0s prediction. We believe this is because the performance of the upstream forecasting module (*i.e.*, our SPCSFNet) in our pipeline does not perform much worse in 3.0s prediction, resulting in that our entire new pipeline performs similarly in 1.0s and 3.0s prediction.

**Visualization.** We visualize the tracking outputs on the predicted scene point cloud (which will be our predicted future trajectories) in Fig. 8, showing that the tracking outputs are very close to the GT, despite that the current upstream module (*i.e.*, SPCSFNet) is not perfect. We expect a higher performance of our new trajectory forecasting pipeline when a better SPCSF solution in the future.

### 6.3 Ablation Study

**Effect of the global scene constraint.** We hypothesize that forecasting the dense scene point cloud can provide a strong constraint on the possible future location of each point and thus reduce the uncertainty of the future. We refer the constraint to as global scene constraint. To justify the hypothesis, we run a variant of our SPCSF on the KITTI dataset by only forecasting a subset of points in a scene point cloud (*e.g.*, points enclosed by the object bounding box). The results are in Table 3. We show that, when only a subset of sparse points is used for forecasting, the performance decreases in both SPCSF and trajectory forecasting. This proves that forecasting a dense scene point cloud can indeed reduce the uncertainty of the future and produce more accurate results

**Effect of the amount of training data.** As our proposed SPCSFNet can be trained with free scene point cloud data without any human annotation, it is useful to know whether the performance of the SPCSFNet can scale with the amount of training data. To that end, we train the SPCSFNet on the KITTI dataset for multiple times with each time we withhold a different number of training sequences. The results are shown in Fig. 9 with two sub-figures in a different  $x$  axis. Clearly, with more training sequences (i.e., more training samples), the performance is increased consistently. Therefore, we can further increase the performance of our SPCSFNet with more training data in the future.

## 7 Conclusion

We propose a new forecasting task, SPCSF, and method SPCSFNet, which predict the densest-possible 3D representation of the future and do not need any human annotation for training. We show that the new task benefits existing downstream tasks by constructing a simple SPCSFNet-based object trajectory forecasting pipeline that achieves state-of-the-art performance.

## References

1. Alahi, A., Goel, K., Ramanathan, V., Robicquet, A., Fei-Fei, L., Savarese, S.: Social LSTM: Human Trajectory Prediction in Crowded Spaces. CVPR (2016)
2. Besl, P., McKay, N.: A Method for Registration of 3-D Shapes. TPAMI (1992)
3. Byravan, A., Fox, D.: Se3-nets: Learning rigid body motion using deep neural networks. ICRA (2017)
4. Caccia, L., Herke Van Hoof, Courville, A., Pineau, J.: Deep Generative Modeling of LiDAR Data. IROS (2019)
5. Caesar, H., Bankiti, V., Lang, A.H., Vora, S., Liong, V.E., Xu, Q.: nuScenes: A Multimodal Dataset for Autonomous Driving. arXiv:1903.11027 (2019)
6. Cao, Y., Barrett, D., Barbu, A., Narayanaswamy, S., Yu, H., Michaux, A., Lin, Y., Dickinson, S., Siskind, J.M., Wang, S.: Recognize Human Activities from Partially Observed Bideos. CVPR (2013)
7. Casas, S., Luo, W., Urtasun, R.: IntentNet: Learning to Predict Intention from Raw Sensor Data. CoRL (2018)
8. Chandra, R., Bhattacharya, U., Bera, A., Manocha, D.: TraPHic: Trajectory Prediction in Dense and Heterogeneous Traffic Using Weighted Interactions. CVPR (2019)
9. Chang, A.X., Funkhouser, T., Guibas, L., Hanrahan, P., Huang, Q., Li, Z., Savarese, S., Savva, M., Song, S., Su, H., Xiao, J., Yi, L., Yu, F.: ShapeNet: An Information-Rich 3D Model Repository. arXiv:1512.03012 (2015)
10. Chang, M.f., Lambert, J., Sangkloy, P., Singh, J., Slawomir, B., Hartnett, A., Wang, D., Carr, P., Lucey, S., Ramanan, D., Hays, J.: Argoverse: 3D Tracking and Forecasting with Rich Maps. CVPR (2019)
11. Deo, N., Trivedi, M.M.: Convolutional Social Pooling for Vehicle Trajectory Prediction. CVPRW (2018)
12. Dou, J., Xue, J., Fang, J.: SEG-VoxelNet for 3D Vehicle Detection from RGB and LiDAR Data. ICRA (2019)
13. Dwyer, B.: A Popular Self-Driving Car Dataset is Missing Labels for Hundreds of Pedestrians, <https://blog.roboflow.ai/self-driving-car-dataset-missing-pedestrians/>

14. Ebert, F., Efros, A.A.: Time-Agonistic Prediction: Predicting Predictable Video Frames. ICLR (2019)
15. Everingham, M., Van Gool, L., Williams, C.K., Winn, J., Zisserman, A.: The Pascal Visual Object Classes (VOC) Challenge. IJCV (2010)
16. Fan, H., Su, H., Guibas, L.: A Point Set Generation Network for 3D Object Reconstruction from a Single Image. CVPR (2017)
17. Fan, H., Yang, Y.: PointRNN: Point Recurrent Neural Network for Moving Point Cloud Processing. arXiv:1910.08287 (2019)
18. Fan, H., Zhu, L., Yang, Y.: Cubic LSTMs for Video Prediction. AAAI (2019)
19. Fisac, J.F., Bronstein, E., Stefansson, E., Sadigh, D., Sastry, S.S., Dragan, A.D.: Hierarchical Game-Theoretic Planning for Autonomous Vehicles. ICRA (2019)
20. Geiger, A., Lenz, P., Urtasun, R.: Are We Ready for Autonomous Driving? the KITTI Vision Benchmark Suite. CVPR (2012)
21. Gupta, A., Johnson, J., Fei-Fei, L., Savarese, S., Alahi, A.: Social GAN: Socially Acceptable Trajectories with Generative Adversarial Networks. CVPR (2018)
22. Hochreiter, S., Schmidhuber, J.: Long Short-Term Memory. Neural Computation (1997)
23. Insaftudinov, E., Dosovitskiy, A.: Unsupervised Learning of Shape and Pose with Differentiable Point Clouds. NeurIPS (2018)
24. Ivanovic, B., Pavone, M.: The Trajectron: Probabilistic Multi-Agent Trajectory Modeling With Dynamic Spatiotemporal Graphs. ICCV (2019)
25. Jin, P., Ohn-bar, E., Kitani, K., Asakawa, C.: A-EXP4: Online Social Policy Learning for Adaptive Robot-Pedestrian Interaction. IROS (2019)
26. Jingwei Xu, Bingbing Ni, Zefan Li, Shuo Cheng, X.Y.: Structure Preserving Video Prediction. CVPR (2018)
27. Kayukawa, S., Kitani, K.: BBeep: A Sonic Collision Avoidance System for Blind Travellers and Nearby Pedestrians. CHI (2019)
28. Kingma, D.P., Ba, J.L.: Adam: A Method for Stochastic Optimization. ICLR (2015)
29. Kitani, K.M., Ziebart, B.D., Bagnell, J.A., Hebert, M.: Activity Forecasting. ECCV (2012)
30. Klovov, R., Verbeek, J., Boyer, E.: Probabilistic Reconstruction Networks for 3D Shape Inference from a Single Image. BMVC (2019)
31. Koppula, H.S., Saxena, A.: Anticipating Human Activities Using Object Affordances for Reactive Robotic Response. TPAMI (2016)
32. Kosaraju, V., Sadeghian, A., Martín-Martín, R., Reid, I., Rezatofighi, S.H., Savarese, S.: Social-BiGAT: Multimodal Trajectory Forecasting using Bicycle-GAN and Graph Attention Networks. NeurIPS (2019)
33. Ku, J., Mozifian, M., Lee, J., Harakeh, A., Waslander, S.: Joint 3D Proposal Generation and Object Detection from View Aggregation. IROS (2018)
34. Lan, T., Chen, T.C., Savarese, S.: A Hierarchical Representation for Future Action Prediction. ECCV (2014)
35. Lang, A.H., Vora, S., Caesar, H., Zhou, L., Yang, J., Beijbom, O.: PointPillars: Fast Encoders for Object Detection from Point Clouds. CVPR (2019)
36. Lee, N., Choi, W., Vernaza, P., Choy, C.B., Torr, P.H., Chandraker, M.: DESIRE: Distant Future Prediction in Dynamic Scenes with Interacting Agents. CVPR (2017)
37. Li, X., Ying, X., Chuah, M.C.: GRIP: Graph-Based Interaction-Aware Trajectory Prediction. ITSC (2019)
38. Liang, M., Yang, B., Wang, S., Urtasun, R.: Deep Continuous Fusion for Multi-Sensor 3D Object Detection. ECCV (2018)

39. Lin, C.H., Kong, C., Lucey, S.: Learning Efficient Point Cloud Generation for Dense 3D Object Reconstruction. AAAI (2018)
40. Liu, X., Qi, C.R., Guibas, L.J.: FlowNet3D: Learning Scene Flow in 3D Point Clouds. CVPR (2019)
41. Luo, W., Yang, B., Urtasun, R.: Fast and Furious: Real Time End-to-End 3D Detection, Tracking and Motion Forecasting with a Single Convolutional Net. CVPR (2018)
42. Mahjourian, R., Wicke, M., Angelova, A.: Geometry-Based Next Frame Prediction from Monocular Video. IV (2017)
43. Manglik, A., Weng, X., Ohn-bar, E., Kitani, K.M.: Future Near-Collision Prediction from Monocular Video: Feasibility, Dataset, and Challenges. IROS (2019)
44. Oliu, M., Selva, J., Escalera, S.: Folded Recurrent Neural Networks for Future Video Prediction. ECCV (2018)
45. Qi, C.R., Su, H., Mo, K., Guibas, L.J.: PointNet: Deep Learning on Point Sets for 3D Classification and Segmentation. CVPR (2017)
46. Qi, X., Liu, Z., corporation Qifeng Chen, D., Jia CUHK, J., Lab, Y.: 3D Motion Decomposition for RGBD Future Dynamic Scene Synthesis. CVPR (2019)
47. Reda, F.A., Liu, G., Shih, K.J., Kirby, R., Barker, J., Tarjan, D., Tao, A., Catanzaro, B.: SDC-Net: Video Prediction Using Spatially-Displaced Convolution. ECCV (2018)
48. Rhinehart, N., Kitani, K.M.: First-Person Activity Forecasting from Video with Online Inverse Reinforcement Learning. TPAMI (2018)
49. Rhinehart, N., Kris, M., Vernaza, P.: R2P2: A Reparameterized Pushforward Policy for Diverse, Precise Generative Path Forecasting. ECCV (2018)
50. Rhinehart, N., McAllister, R., Kitani, K., Levine, S.: PRECOG: PREDiction Conditioned On Goals in Visual Multi-Agent Settings. ICCV (2019)
51. Robicquet, A., Sadeghian, A., Alahi, A., Savarese, S.: Learning Social Etiquette: Human Trajectory Understanding In Crowded Scenes. ECCV (2016)
52. Rubner, Y., Tomasi, C., Guibas, L.J.: The Earth Mover's Distance as a Metric for Image Retrieval. IJCV (2000)
53. Rudenko, A., Palmieri, L., Herman, M., Kitani, K.M., Gavrila, D.M., Arras, K.O.: Human Motion Trajectory Prediction: A Survey. arXiv:1905.06113 (2019)
54. Sadeghian, A., Kosaraju, V., Sadeghian, A., Hirose, N., Rezaatoughi, S.H., Savarese, S.: SoPhie: An Attentive GAN for Predicting Paths Compliant to Social and Physical Constraints. CVPR (2018)
55. Shi, S., Wang, X., Li, H.: PointRCNN: 3D Object Proposal Generation and Detection from Point Cloud. CVPR (2019)
56. Shu, D.W., Park, S.W., Kwon, J.: 3D Point Cloud Generative Adversarial Network Based on Tree Structured Graph Convolutions. ICCV (2019)
57. StypuÅłkowski, M., Zamorski, M., ZiÅłba, M., Chorowski, J.: Conditional Invertible Flow for Point Cloud Generation. NeurIPS (2019)
58. Tomasello, P., Sidhu, S., Shen, A., Moskewicz, M.W., Redmon, N., Joshi, G., Phadte, R., Jain, P., Iandola, F.N.: DSCnet: Replicating LiDAR Point Clouds with Deep Sensor Cloning. CVPRW (2019)
59. Vitus, M.P., Tomlin, C.J.: A Probabilistic Approach to Planning and Control in Autonomous Urban Driving. CDC (2013)
60. W Kuhn, H.: The Hungarian Method for the Assignment Problem. Naval Research Logistics Quarterly (1955)
61. Walker, J., Marino, K., Mulam, H., Hebert, M.: The Pose Knows: Video Forecasting by Generating Pose Futures. ICCV (2017)

62. Wang, S., Jia, D., Weng, X.: Deep Reinforcement Learning for Autonomous Driving. arXiv:1811.11329 (2018)
63. Wang, Y., Solomon, J.M.: Deep Closest Point: Learning Representations for Point Cloud Registration. ICCV (2019)
64. Weng, X., Kitani, K.: A Baseline for 3D Multi-Object Tracking. arXiv:1907.03961 (2019)
65. Weng, X., Kitani, K.: Monocular 3D Object Detection with Pseudo-LiDAR Point Cloud. arXiv:1903.09847 (2019)
66. Weng, X., Yuan, Y., Kitani, K.: Joint 3D Tracking and Forecasting with Graph Neural Network and Diversity Sampling. arXiv:2003.07847 (2020)
67. Yang, B., Luo, W., Urtasun, R.: PIXOR: Real-time 3D Object Detection from Point Clouds. CVPR (2018)
68. Yang, G., Huang, X., Hao, Z., Liu, M.Y., Belongie, S., Hariharan, B.: PointFlow: 3D Point Cloud Generation with Continuous Normalizing Flows. ICCV (2019)
69. Yuan, W., Khot, T., Held, D., Mertz, C., Hebert, M.: PCN: Point Completion Network. 3DV (2018)
70. Zeng, W., Luo, W., Suo, S., Sadat, A., Yang, B., Casas, S., Urtasun, R.: End-to-End Interpretable Neural Motion Planner. CVPR (2019)
71. Zhou, T., Brown, M., Noah, G., Google, S., Lowe Google, D.G.: Unsupervised Learning of Depth and Ego-Motion from Video. CVPR (2017)
72. Zhou, Y., Tuzel, O.: VoxelNet: End-to-End Learning for Point Cloud Based 3D Object Detection. CVPR (2018)

## A Matching in New Trajectory Evaluation

As mentioned in Section 5 for our proposed evaluation procedure, we match the predicted future trajectories and future GT trajectories using the Hungarian algorithm in order to compute the error metrics. Specifically, we first compute the pairwise ADE between every possible pair of predicted and GT future trajectories. For example, if we have  $U$  predicted and  $V$  GT future trajectories, we will obtain a  $U \times V$  matrix with each entry being the ADE for the pair of GT and predicted trajectories. Note that, for the GT trajectories that are incomplete in the future  $N$  frames, we mask out the missing frames and still use the trajectories that are partially available to compute the ADE. Then, the obtained ADE matrix will be fed to the Hungarian algorithm to obtain a one-to-one correspondence between the predicted and GT trajectories. As a result, the trajectories that have the correspondences (i.e., matched) are considered as true positives, and the unmatched predicted trajectories and the unmatched GT trajectories will be the false positives and false negatives respectively, all of which will be used to compute every operating point in the ADE-over-recall and FDE-over-recall curves and finally compute the AADE/AFDE metrics through integration. To approximate the integration, we use the values of ADE/FDE at a maximum of 40 recall values linearly distributed between 0% and 100% to compute the AADE/AFDE. Note that not all 40 (i.e. with an interval of recall of 2.5%) operating points are used in our experiments, we only integrate the ADE/FDE values up to the recall value that all methods can reach. For example, in Fig. 7 (right) of the main paper, the recall that all three methods can reach is 0.425. If we only compare these three methods, we will integrate the ADE/FDE for all

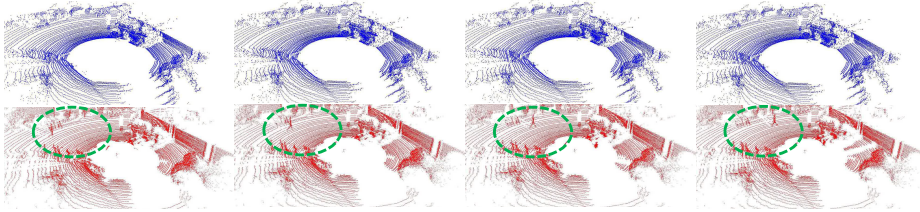


**Fig. 10: Failure Cases: (Top)** Our predicted future scene point cloud; **(Bottom)** GT future scene point cloud. We draw a green ellipse in the GT future scene point cloud to enclose a walking pedestrian which does not seem to be reconstructed in our predicted future scene point cloud. 4 frames of results are chosen from a sample prediction of 30 future frames (i.e. 3 seconds prediction setting) in KITTI.

three methods at the recall values from 0.025, 0.050,  $\dots$ , to 0.425. For results in Table 2 of the main paper, the recall values that are used to compute the integral metrics are different across settings.

## B Training Details

We train the entire network using the Adam [28] optimizer for 30 epochs with a learning rate of  $1 \times 10^{-4}$  and betas of 0.9 and 0.999. We use the  $\lambda_1$  of 0.1 and  $\lambda_2$  of 0.1 for the loss in the Eq. (1).

## C Failure Cases

Although the predicted scene point cloud by our SPCSFNet can reasonably reconstructs the scene structure and large objects (e.g., vehicles) as shown in Fig. 8 of the main paper, our current model does not seem to be able to reconstruct the small objects in the scene (e.g., pedestrians) and capture their motion as shown in Fig. 10 of this file, which is the main limitation of our current method. We believe it is because that the latent feature in SPCSFNet with dimensionality of 1024 only contains limited amount of information which is dominated by the scene structure and motion of large objects, is thus not able to preserve fine-grained information for small objects. To deal with this issue, we will keep updating our method in the short future in order to achieve fine-grained reconstruction, e.g., replace convolution with dilated convolution, add multi-scale feature learning, add residual connection, etc.